The lncRNA *APOLO* interacts with the transcription factor WRKY42 to trigger root hair cell expansion in response to cold

Michaël Moison[*1], Javier Martínez Pacheco[*2], Leandro Lucero[*1], Camille Fonouni-Farde[1], Johan Rodríguez-Melo[3], Aurélie Christ[4], Jérémie Bazin[4]; Moussa Benhamed[4]; Fernando Ibañez[3], Martin Crespi[4], José M. Estevez[†,2,5] and Federico Ariel[†1]

[1] Instituto de Agrobiotecnología del Litoral, Universidad Nacional del Litoral, CONICET, FBCB, Centro Científico Tecnológico CONICET Santa Fe, Colectora Ruta Nacional No 168 km. 0, Paraje El Pozo, Santa Fe 3000, Argentina.

[2] Fundación Instituto Leloir and IIBBA-CONICET, Av. Patricias Argentinas 435, Buenos Aires CP C1405BWE, Argentina.

[3] Instituto de Investigaciones Agrobiotecnológicas, CONICET, Universidad Nacional de Río Cuarto, Río Cuarto 5800, Argentina.

[4] Institute of Plant Sciences Paris-Saclay (IPS2), CNRS, INRA, University Paris-Saclay and University of Paris Bâtiment 630, 91192 Gif sur Yvette, France.

[5] Centro de Biotecnología Vegetal (CBV), Facultad de Ciencias de la Vida (FCsV), Universidad Andrés Bello, Santiago, Chile and Millennium Institute for Integrative Biology (iBio), Santiago, Chile.

[*] These authors contributed equally to this work

[†] Correspondence to: Federico Ariel (fariel@santafe-conicet.gov.ar) and José M. Estevez (jestevez@leloir.org.ar)

Text Word count (without Abstract and References)**:** 4,984

ABSTRACT

Plant long noncoding RNAs (lncRNAs) have emerged as important regulators of chromatin dynamics, impacting on transcriptional programs leading to different developmental outputs. The lncRNA *AUXIN REGULATED PROMOTER LOOP* (*APOLO*) directly recognizes multiple independent loci across the *Arabidopsis* genome and modulates their three-dimensional chromatin conformation, leading to transcriptional shifts. Here, we show that *APOLO* recognizes the locus encoding the root hair (RH) master regulator ROOT HAIR DEFECTIVE 6 (RHD6) and controls *RHD6* transcriptional activity leading to cold-enhanced RH elongation, in association with the Polycomb Repressive Complexes (PRC) 1 and 2. Additionally, we demonstrate that *APOLO* interacts with the transcription factor WRKY42 and modulates its binding to the *RHD6* promoter. WRKY42 is required for the activation of *RHD6* by low temperatures and *WRKY42* deregulation impairs cold-induced RH expansion. Collectively, our results indicate that a novel ribonucleoprotein complex involving *APOLO* and WRKY42 forms a regulatory hub which activates *RHD6* by shaping its epigenetic environment and integrates different signals governing RH growth and development.

Words: 160

Key words: root hairs; cell expansion; long noncoding RNAs; *APOLO*; transcription factors; RHD6; WRKY42; cold

INTRODUCTION

Root hairs (RHs) are single cell projections developed from specialized epidermal trichoblast cells able to increase their size several hundred times in a polar manner to reach and promote the uptake of water-soluble nutrients, interact with microorganisms and anchor the plant to the soil. The specification of epidermal cells into RHs involves a cell fate determination process whose underlying mechanisms are only partially understood. In *Arabidopsis thaliana*, RH cell fate is controlled by a developmental program involving a complex of transcription factors (TFs) promoting the expression of the homeodomain protein GLABRA 2 (GL2)(1–4). GL2 blocks RH development by inhibiting the transcription of the master regulator *ROOT HAIR DEFECTIVE 6* (*RHD6*)(5). In the trichoblast cells that differentiate into RHs, a second TF complex suppresses *GL2* expression (3), forcing the cells to enter the RH cell fate program via the concomitant activation of RHD6 along with downstream TFs (6,7). Briefly, RHD6 together with its homolog RHD6-LIKE 1 (RSL1) induce the expression of other TFs from the bHLH family, including RSL2 and RSL4, ultimately triggering the differentiation of the RHs and their subsequent polarized tip-growth (8–10). In addition, it was proposed that RSL4 controls the expression of a small subset of nearly 125 genes (9, 11–13), including several cell wall extensins (*EXTs*) (14, 15) sufficient to promote RH growth (16).

RH expansion is regulated both by cell-intrinsic factors (e.g. endogenous phytohormones such as auxin) and external environmental signals (e.g. phosphate (Pi) availability in the soil) (17, 18). Pi starvation is one of the key environmental factors promoting rapid RH growth (9, 12, 13). In *Arabidopsis*, it triggers *RSL4* expression via an enhanced auxin production, activating downstream effector genes mediating cell growth (9, 12, 17-19). Accordingly, several auxin-related TFs have been implicated in Pi-starvation signaling in roots, including WRKY proteins that control the expression of the Pi transporter families Pi-permease PHO1 and PHOSPHATE TRANSPORTER (PHT) (20–23). Under Pi-sufficient conditions, WRKY6 and WRKY42 bind to W-boxes of the *PHO1* promoter and suppress its expression. During Pi starvation, WRKY42 is degraded by the 26S proteasome pathway, resulting in the activation of *PHO1* transcription (21, 23). In addition, WRKY42 functions as a positive regulator of *PHT1;1*, by binding to its promoter under Pi-sufficient condition (23). Overall, WRKY42 is part of the components activating root early-responses to Pi starvation, although its role in controlling RH growth remains unexplored.

In recent years, plant long noncoding RNAs (lncRNAs) have emerged as important regulators of gene expression, and several among them have been functionally linked to Pi homeostasis. For instance, the lncRNA *INDUCED BY PHOSPHATE STARVATION 1* (*IPS1*) can sequester the Pi starvation-induced microRNA miR-399, attenuating miR-399-mediated repression of *PHO2*, a gene involved in Pi uptake (24). In

addition, the *cis*-natural antisense (*cis*-NAT) transcript *PHO1;2*, induced under Pi deficiency, was shown to promote the translation of the *PHO1;2* mRNA involved in Pi loading into the xylem. The expression of this *cis*-NAT is associated with the transport of the sense–antisense RNA pair toward the polysomes (25). More recently, it was shown that the lncRNA *AUXIN REGULATED PROMOTER LOOP* (*APOLO*) recognizes multiple spatially independent genes by sequence complementarity and DNA-RNA duplex formation, known as R-loops. Upon recognition, *APOLO* shapes the three-dimensional (3D) conformation of its target regions by decoying the Polycomb Repressive Complex 1 (PRC1) component LIKE HETEROCHROMATIN PROTEIN 1 (LHP1), thereby regulating their transcription (26, 27).

Here, we show that the lncRNA *APOLO* directly regulates a subset of genes involved in RH development, including the master regulator of RH initiation *RHD6*. *APOLO* activates *RHD6* transcription by modulating the formation of a local chromatin loop encompassing its promoter region, an epigenetic regulatory mechanism likely involving PRC1 and PRC2 components. Furthermore, we found that *APOLO* interacts with the TF WRKY42, forming a new hub that regulates *RHD6* to induce RH growth in response to low temperatures.

RESULTS

APOLO regulates root hair cell elongation in response to low temperatures

The lncRNA *APOLO* was previously reported to recognize a subset of independent loci enriched in categories related to cell wall composition and organization (27). A closer look at *APOLO bona fide* targets allowed us to identify seventeen genes involved in RH growth and expansion (**Supplementary Table 1**), a process dependent on cell wall remodeling molecules, including EXTs and EXT-related proteins (14, 15, 28–30). Interestingly, according to single-cell RNA-seq datasets (31) *APOLO* transcripts are enriched in RH cells (**Supplementary Figure 1**). Notably, sixteen *APOLO* direct targets were upregulated and one downregulated (*EXT18*) upon *APOLO* over-expression (**Supplementary Table 2**). Furthermore, 52 additional RH-related genes were upregulated in *35S:APOLO* seedlings, albeit not identified as *APOLO* direct targets (**Supplementary Table 2**) (27). Among them, the RH central TF genes *RHD6* (as a direct target), *RSL2* and *RSL4* (as indirectly regulated) were induced upon *APOLO* over-expression.

It was reported that the *APOLO* locus is targeted by the RNA-polymerase Pol V and silenced by RNA-directed DNA Methylation (RdDM, (26)). A search in a small RNA-Seq performed in WT roots subjected to different temperature treatments (32) revealed that RdDM-related 24nt siRNA accumulation over the *APOLO* locus is less abundant at low temperatures (15°C; **Figure 1A**), suggesting that *APOLO*

transcription is regulated by cold. Accordingly, we found that *APOLO* transcriptional accumulation increases in roots after 24h at 10°C (**Figure 1B**). An analysis of the promoter activity of the 5.2kb region upstream *APOLO* (27) directing the expression of a *GFP* reporter gene, additionally revealed a higher transcriptional activity at low temperatures in the RHs (**Figure 1C**). Strikingly, we observed that two RNAi-*APOLO* and two *35S:APOLO* independent lines (26, 27) exhibit a basal increase of RH length at 22°C, and uncovered a strong induction of RH elongation in WT and RNAi-*APOLO* at 10°C, in contrast to *35S:APOLO* lines (**Figure 1D**). Accordingly, *RHD6* is induced in response to cold in WT roots and RNAi-*APOLO* roots display higher *RHD6* basal levels than the WT (**Figure 1E**). Collectively, our findings suggest that *APOLO* participates in the induction of cold-mediated RH elongation and that a deregulation of *APOLO* transcript levels can impact RH growth.

Previous studies pointed out a key role of RHD6 (together with RSL1) in RH development, which is mediated by RSL4 and RSL2 as downstream regulators of RH cell elongation (6, 7). Considering that *RHD6*, *RSL2* and *RSL4* transcript levels were upregulated in *35S:APOLO* seedlings (**Supplementary Table 2**; (27)), we assessed if these TFs were also controlling the promotion of RH growth by low temperatures. To this end, we tested how *rhd6/rsl1/rsl4* and *rsl2*, *rsl4* and double mutant plants *rsl2/rsl4* respond to low temperatures in comparison with control conditions. The *rsl2* mutant was highly responsive to low temperatures in a similar manner to WT while *rsl4* was impaired in the response to cold. The double mutant *rsl2/rsl4* and the triple mutant *rhd6/rsl1/rsl4* did not develop RHs in either of the two conditions (**Supplementary Figure 2A**). In addition, constitutive expression of *RSL4* (*35S:RSL4*) as well as its expression under the control of the RH specific *EXPANSIN7* promoter (*EXP7p:RSL4*) boosted basal RH growth without further enhancement in response to cold (**Supplementary Figure 2B**). These results demonstrate that RSL4 is largely required for RHD6-dependent activation of RH growth at low temperatures, and RSL2 might participate to a lower extent.

APOLO* directly modulates the three-dimensional chromatin conformation of the root hair specific locus *RHD6

Among *APOLO* targets involved in RH development, we found the master regulator of RH initiation *RHD6* (6, 7). The epigenetic profile of the *RHD6* locus corresponds to typical *APOLO* targets (**Figure 2A**, (27)), including H3K27me3 deposition (track 1), LHP1 recognition (track 2, chromatin immunoprecipitation (ChIP)-Seq, (33)), and *APOLO* binding regions (tracks 3 to 5, chromatin isolation by RNA purification (ChIRP)-Seq, (27)). A GAAGAA box, shown to be important for *APOLO* target recognition (27) is located in the *RHD6* locus and coincides with *APOLO* binding site. In addition, a small peak indi-

cates the presence of an R-loop coinciding with *APOLO* recognition sites over *RHD6* (tracks 6 to 9, DNA-RNA hybrid immunoprecipitation (DRIP)-Seq (34)). The possibility that *RHD6* recognition by *APOLO* occurs specifically in RHs may explain the dilution of the signal coming from entire seedlings (34).

Remarkably, *APOLO* recognition and R-loop formation are also detectable over *RHD6* neighbor gene, located 3.2 kb upstream *RHD6* transcription start site (**Figure 2A**). According to *Dpn*II Hi-C datasets from Arabidopsis seedlings (35), a chromatin loop encompassing the intergenic region upstream *RHD6* was detected (**Figure 2B**), exhibiting *APOLO* binding at both sides of the loop base (**Figure 2A**, ChIRP-Seq). By performing a ChIRP-qPCR with two independent sets of biotinylated probes to purify *APOLO* (ODD and EVEN; (27)) and one additional set used as a negative control (LacZ), we confirmed that *APOLO* RNA–*RHD6* DNA interaction occurs in wild-type (WT) and is lost in *APOLO* knockdown (RNAi) seedlings ((26); **Figure 2C**). In addition, the quantification of relative *RHD6* loop formation in RNAi-*APOLO* and *APOLO* over-expressing (*35S:APOLO*; (27)) seedlings, revealed impaired loop formation in both lines (**Figure 2D**), hinting at a stoichiometric requirement of *APOLO* for *RHD6* chromatin loop formation. Accordingly, an RNA-Seq dataset of *35S:APOLO* seedlings *vs.* WT (27) indicates that *RHD6* transcript levels are increased upon *APOLO* over-expression (**Figure 2E, Supplementary Table 1**), suggesting that the chromatin loop including *RHD6* promoter region precludes transcription. Altogether, our results indicate that *APOLO* lncRNA directly regulates *RHD6* transcriptional activity by fine-tuning local chromatin 3D conformation.

It was previously reported that PRC2 actively participates in the regulation of RH growth (36) and that the *RHD6* locus exhibits H3K27me3 deposition and LHP1 recognition (**Figure 2A;** (33)). Thus, we decided to explore the role of PRC1 and 2 in *APOLO*-mediated *RHD6* activation at low temperatures. At 22°C, *RHD6* suffers a reduction of H3K27me3 in the PRC2 mutant *curly leaf* (*clf*), in contrast to the PRC1 mutant *lhp1* (**Supplementary Figure 3A;** (33)). Interestingly, we observed that H3K27me3 deposition and LHP1 binding diminish in WT roots treated for 24h at 10°C compared to 22°C (**Supplementary Figure 3B**), in agreement with the induction of *RHD6* in response to cold (**Figure 2E**). Moreover, *lhp1* and *clf* mutants exhibit a basal decrease of RH length together with a slight decrease of cold-induced RH elongation in *lhp1*, and a strong decrease of cold-induced RH elongation in *clf* (**Supplementary Figure 3D**). Consistently, *RHD6* transcriptional activation by cold is abolished in the *clf* mutant (**Supplementary Figure 3C**), hinting at an important role of chromatin rearrangement for *RHD6* activation in response to cold.

APOLO* interacts with the transcription factor WRKY42 to coordinate the activation of *RHD6

With the aim of identifying novel actors involved in cold-induced transcriptional regulation of RH growth, we analyzed the sequence of the promoter regions of RH-related *APOLO* targets. Notably, 13 out

of the 17 *APOLO* targets contained between 1 and 4 canonical WRKY TF binding sites (W-box) in their promoters, including *RHD6* (**Supplementary Table 1**). According to the Arabidopsis eFP Browser (37), the TF-encoding gene *WRKY42* is induced in roots when seedlings are subjected to 4°C for 24h (**Figure 3A**). Remarkably, WRKY42 is involved in the response to Pi starvation (23), an environmental condition that promotes RH cell expansion (18) in a similar manner to low temperatures. At 10°C, we observed that *WRKY42* transcriptional accumulation augments significantly in roots (**Figure 3B**). By using a *35S:WRKY42:GFP* line, we demonstrated that WRKY42 can directly bind to the promoter region of *RHD6* (**Figure 3C**). Accordingly, the over-expression of *WRKY42* (*35S:WRKY42:GFP* line) led to a basal increase of *RHD6* levels (**Figure 3D**) and RH elongation (**Figure 3E**) at ambient temperature, mimicking the effect of cold. On the contrary, cold-mediated induction of *RHD6* is abolished in the *wrky42* mutant (23; **Figure 3D**), which consistently exhibits shorter RHs at 22°C and partially impaired RH elongation at low temperatures (**Figure 3E**). Taken together, our results suggest that WRKY42 is an important regulator of *RHD6*-mediated RH growth in response to cold.

We thus wondered to what extent WRKY42 regulates the epigenetic landscape of the *RHD6* locus. We first observed that H3K27me3 deposition over *RHD6* is significantly augmented in the *wrky42* mutant background, in contrast to *AZG2*, an *APOLO* target non-related to WRKY42 (**Figure 4A**), consistent with reduced *RHD6* basal levels reported in *wrky42* (**Figure 3D**). Considering that other TFs were shown to directly interact with lncRNAs in animals (38-40), we wondered if WRKY42 can recognize *APOLO in planta*. Thus, *APOLO*-WRKY42 interaction was assessed and validated by RNA immunoprecipitation (RIP-qPCR) in tobacco leaves and in *Arabidopsis* plants transitory or stably transformed with 35S:*WRKY42:GFP*, respectively (**Figure 4B**). Therefore, we evaluated the mutual contribution of *APOLO* and WRKY42 to their respective recognition of the *RHD6* locus. *APOLO* ChIRP-qPCR in the WT and *wrky42* mutant (**Figure 4C**) revealed similar binding to *RHD6*, indicating that WRKY42 does not participates in *APOLO*-target recognition. Reciprocally, we assessed the control of *APOLO* over WRKY42 recognition of the *RHD6* locus. To this end, chromatin was extracted from *35S:WRKY42:GFP* seedlings and increasing amounts of *in vitro* transcribed *APOLO* were added before cross-link and regular WRKY42 ChIP over *RHD6*. Strikingly, increasing concentrations of *APOLO* gradually decoy WRKY42 away from the *RHD6* locus (**Figure 4D**), hinting at a stoichiometric regulation of *APOLO* over the activity of its partner TF.

Collectively, our results indicate that the regulation of *RHD6* expression in response to cold depends on Polycomb-dependent H3K27me3 dynamic deposition. The WRKY42-*APOLO* complex modulates the epigenetic environment of *RHD6*, activating its transcription and promoting RH growth at

low temperatures. *RHD6* activation further triggers the expression of *RSL2* and *RSL4* that control the transcriptional RH program inducing cell expansion in response to cold (**Figure 4E**).

DISCUSSION

Cell fate determination in the epidermis has been extensively studied (1–4). Once trichoblast cells differentiate in the root epidermis, RHs develop as fast polar growing protuberances in response to endogenous and environmental signals (6, 7, 9, 19). RHs are one of the main entry points in the roots for water-soluble macronutrients, such as Pi and nitrates. Pi is an essential element for plant growth and development, and the availability of this macronutrient is a factor limiting plant productivity. Low Pi in the soil triggers auxin synthesis and transport in Arabidopsis roots, enhancing RH elongation to promote Pi uptake (18). Thus, auxin mediates low Pi-induced promotion of RH cell expansion. Under low soil Pi, auxin synthesis is enhanced specifically in the root cap (41) and transported (mostly by AUX1, PIN2, and PGP4) from the apex to the differentiation zone, specifically leading to an increase of auxin levels in trichoblasts (18, 42, 43). In response to the high-auxin microenvironment, RHs protrude from the root epidermis controlled by RHD6 and RSL1 (6, 7). High levels of auxin in trichoblasts trigger a signaling cascade mediated by TIR1-ARF19 (and possibly also ARF7) that directly induce the expression of *RSL4* (and likely of *RSL2*) and promote RH elongation (9, 17, 18, 44). ARF7 and ARF19 also activate other RH genes independently of RSL4 (45). Interestingly, our results indicate that the lncRNA *APOLO* participates in the response to low temperatures. *APOLO* is directly activated by ARF7 and regulates the transcriptional activity of its neighboring gene *PINOID* (*PID*) by shaping local 3D chromatin conformation (26, 27). *PID* encodes a kinase responsible for accurate auxin polar transport by localizing PIN2 in the root cell membrane (46). More recently, it was shown that *APOLO* can recognize a subset of distant genes across the *Arabidopsis* genome, most of them being related to auxin synthesis and signaling (27). In this work, we demonstrate that a group of RH related genes are directly regulated by *APOLO* in response to cold, including the RH master regulator *RHD6*. Collectively, our results uncover a lncRNA-mediated epigenetic link between environmental signals and auxin homeostasis modulating RH growth.

As mentioned above, nutrient availability is known to activate RH expansion through a transcriptional reprogramming governed by RHD6 and downstream TFs. The quantification of RH growth of WT plants in response to increasing concentrations of nutrients (0.5X to 2.0X MS (Murashige and Skoog) medium) indicates that high concentrations of nutrients completely abolish RH growth triggered by low temperatures **(Supplementary Figure 4A**). In a similar way, by increasing agar concentration in the MS medium (from 0.8% to 2.5%) restraining nutrient mobility, cold-induced RH is clearly blocked **(Supple-**

mentary Figure 4B). Altogether, these observations suggest that low temperatures may restrict nutrient mobility and availability in the culture medium, leading to the promotion of polar RH growth. Further research will be needed to determine what is the limiting nutrient mediating the effect of cold on RH growth.

Although substantial progress has been achieved in the identification of the molecular actors that control RH development, the impact of chromatin conformation in the transcriptional regulation of central TFs remains poorly understood. In this study, we have revealed a new mechanism of gene regulation in RHs by which the lncRNA *APOLO* integrates chromatin-associated ribonucleoprotein complexes together with the TF WYRK42, participating in the transcriptional activation of *RHD6* and the downstream RH gene network (**Figure 4D**). *APOLO* directly regulates the chromatin 3D conformation of the genomic region encompassing the *RHD6* locus and stoichiometrically recruits WYRK42, previously linked to Pi-starvation (21, 23). Our results suggest that an *APOLO*-WRKY42 hub regulates RH cell elongation through the master regulator RHD6, although the *APOLO*-WYRKY42 hub potentially targets several additional cell wall related genes (**Supplementary Table 1**) at the end of the pathway controlled by RHD6 and the RHD6-downstream TFs RSL2/RSL4 (17, 47).

Participation of epigenetic factors in root cell identity determination strongly suggests that the default pattern for epidermal cell fate can be overridden by environmental stimuli (48). Interestingly, it was reported that the expression of *GLABRA2* (*GL2*), a gene encoding a TF repressing *RHD6* in atrichoblasts, is tightly regulated at the epigenetic level. By using 3D fluorescence *in situ* hybridization, it was shown that alternative states of chromatin organization around the *GL2* locus are required to control position-dependent cell-type specification in the root epidermis (49). Furthermore, *GL2* epigenetic regulation was proposed to be responsive to salt stress (50). In addition, a comprehensive characterization of alternative mutant lines uncovered the role of PRC2 in the regulation of RH development (36). Loss-of-function mutants in different PRC2 subunits develop unicellular RHs but fail to retain the differentiated state, generating a disorganized cell mass from each single RH. It was shown that the resulting RHs are able to undergo a normal endoreduplication program, increasing their nuclear ploidy, although they subsequently reinitiate mitotic division and successive DNA replication. It was proposed that aberrant RH development in PRC2-related mutants is due to the epigenetic deregulation of key genes such as *WOUND INDUCED DEDIFFERENTIATION 3* (*WIND3*) and *LEAFY COTYLEDON 2* (*LEC2*) (36). Here, we showed that the single mutants *clf* (PRC2) and *lhp1* (PRC1) are affected in RH growth. Moreover, we showed that H3K27me3 deposition throughout the *RHD6* locus is partially impaired in the *clf* background, which is affected in RH elongation promoted by cold. Altogether, our results suggest that

Polycomb proteins participate in the control of RH-related genes transcriptional reprogramming at low temperatures.

Notably, CLF and LHP1 were shown to interact with a subset of lncRNAs in *Arabidopsis*, modulating the activity of PRC target genes (51). Interestingly, several lncRNAs have been linked to the control of transcription in response to cold. *FLOWERING LOCUS C* is regulated by at least three lncRNAs. First, the alternative splicing of a set of antisense transcripts, collectively named as *COOLAIR*, depends on the prolonged exposure to cold, epigenetically repressing *FLC* (52). The use of the *COOLAIR* proximal poly(A) site results in down-regulation of *FLC* expression in a process involving FLOWERING LOCUS D (FLD), an H3K4me2 demethylase (53). A second lncRNA called *COLD ASSISTED INTRONIC NONCODING RNA* (*COLDAIR*) is fully encoded in the first intron of *FLC.* Similar to *COOLAIR*, its accumulation oscillates in response to low temperatures. It was proposed that *COLDAIR* recruits the PRC2 component CLF to target *FLC* for H3K27me3 deposition (54). More recently, a third lncRNA modulating *FLC* transcription was identified (55). The cold-responsive lncRNA *COLDWRAP* is derived from the *FLC* proximal promoter and it also interacts with PRC2. It was suggested that *COLDWRAP* functions in cooperation with the lncRNA *COLDAIR* to retain Polycomb at the *FLC* promoter through the formation of a repressive intragenic chromatin loop (55). Another lncRNA named *SVALKA* was shown to mediate the response to low temperatures (56). Interestingly, the activation of *SVALKA* by cold triggers the transcription of a cryptic downstream lncRNA, which overlaps the antisense locus of the *C-repeat/dehydration-responsive element Binding Factor 1* (*CBF1*), involved in the early response to cold in Arabidopsis. Antisense transcription causes Pol II head-to-head collision modulating transcriptional termination of *CBF1* (56). Here, we showed that the auxin-responsive lncRNA *APOLO* is also transcriptionally modulated by cold. The differential accumulation of 24nt siRNAs across the *APOLO* locus at low temperatures indicates that this activation is related to a decrease in RdDM. Moreover, we showed here that the intergenic region between *PID* and *APOLO* acting as a divergent promoter is also activated at low temperatures in RHs, as revealed by the reporter gene *GFP*. Thus, the lncRNA *APOLO* integrates external signals into auxin-dependent developmental outputs in Arabidopsis.

In the last decade, lncRNAs have emerged as regulators of gene expression at different levels, ranging from epigenetics to protein modifications and stability (57). Notably, it has been shown in animals that noncoding transcripts can be recognized by TFs. In humans, it was proposed that the interaction with the lncRNA *SMALL NUCLEOLAR RNA HOST GENE 15* (*SNHG15*) stabilizes the TF Slug in colon cancer cells. It was shown that *SNHG15* is recognized by the zinc finger domain of Slug preventing its ubiquitination and degradation in living cells (38). Also, the transcriptional activity of the human gene

DIHYDROFOLATE REDUCTASE (*DHFR*) is regulated by a lncRNA encoded in its proximal promoter. It was proposed that the nascent noncoding transcript forms a hybrid with its parent DNA and decoys the regulatory TF IIB away from the *DHFR* promoter, dissociating the transcriptional pre-initiation complex in quiescent cells (40). The lncRNA *P21 ASSOCIATED ncRNA DNA DAMAGE ACTIVATED* (*PANDA*) was identified in human cancer and it was activated in response to DNA damage (39). *PANDA* is transcribed from the promoter region of the *CDKN1A* gene and interacts with the TF NF-YA to limit the expression of pro-apoptotic genes. The activity of *PANDA* has been linked to the progression of different tumors (58, 59). Interestingly, it was shown that in addition to NF-YA, *PANDA* interacts with the scaffold-attachment-factor A (SAFA) as well as PRC1 and PRC2 to modulate cell senescence. In proliferating cells, SAFA and *PANDA* recruit Polycomb components to repress the transcription of senescence-promoting genes. Conversely, the loss of SAFA–PANDA–PRC interactions allows expression of the senescence program (60). In this work, we showed that the PRC1-interacting lncRNA *APOLO* can also be recognized by the TF WRKY42, hinting at general lncRNA-mediated mechanisms linking Polycomb complexes with the transcriptional machinery across kingdoms. Furthermore, our observations indicate that the deregulation of *WRKY42* affects the epigenetic environment of *RHD6*. It was previously shown that the addition of *in vitro* transcribed *APOLO* to RNAi-*APOLO* chromatin extracts was able to partially restore R-loop formation over *APOLO* target genes, and that high levels of *APOLO* may titer LHP1 away from chromatin (27). Here we showed that the relative accumulation of the lncRNA *APOLO* can modulate the binding activity of its partner TF to common target genes. Collectively, our results strongly support that environmentally controlled cell fate in *Arabidopsis* relies on a transcriptional reprogramming governed by a network of epigenetic regulatory complexes, lncRNAs, TFs and effector proteins.

MATERIALS AND METHODS

Plant Material and Growth Conditions. All the *Arabidopsis thaliana* lines used were in the Columbia-0 (Col-0) background. *WRKY42* over expression transgenic plants were generated through *Agrobacterium tumefaciens* (strain EHA105)-mediated transformation (61). *35S:WRKY42:GFP* transformant lines were selected on MS/2 medium supplemented with kanamycin (40µg/mL) and *WRKY42* expression levels were measured by RT-qPCR (primers used are listed in **Supplementary Table 3**). The *wrky42* mutant line belongs to the SALK collection (SALK_121674C), as the one previously characterized (23). Homozygous plants were obtained in our laboratory and genotyped using the oligonucleotides indicated in **Supplementary Table 3**. Seeds were surface sterilized and stratified at 4°C for 2d before being grown under

long day conditions (16h light, 140µE.m^{-2}.sec^{-1}/8h dark), on ½-strength Murashige and Skoog media (1/2 MS) (Duchefa, Netherlands) with 0.8% plant agar (Duchefa, Netherlands).

Cloning procedure. The coding region of *WRKY42* (AT4G04450) excluding the STOP codon was amplified by PCR, cloned into the Gateway entry vector pENTR/D-TOPO (Invitrogen) and recombined by Gateway technology (LR reaction) into the pK7FWG2,0 vector containing a *p35S-GFP* cassette (http://www.psb.ugent.be/gateway/index.php).

Root hair phenotype characterization. For quantitative analyses of RH phenotypes, 100 fully elongated RHs were measured (using the ImageJ software) from 10-20 roots grown on vertical agar plates for 5 days at 22° and 3 days at 10°C. Measurements were made after 8 days. Images were captured with an Olympus SZX7 Zoom Stereo microscope (Olympus, Japan) equipped with a Q-Colors digital camera and software.

Confocal microscopy analysis of root hairs. Confocal laser scanning microscopy was performed using Zeiss LSM5 Pascal (Zeiss, Germany) and a 40x water-immersion objective, N/A=1.2. Fluorescence was analyzed by using 488 nm laser for GFP excitation (Laser Intensity: 70%, Detector Gain:550, Amplifier Offset:0.1, Amplifier Gain:1), and emitted fluorescence was recorded between 490 and 525nm for GFP tag. Z stacks were done with an optical slice of 1µm, and fluorescence intensity was measured in 15µm ROI (Region Of Interest) at the RH tip and summed for quantification of fluorescence using ImageJ. Five replicates for each of ten roots and 15 hairs per root were observed. Col-0 wild type root hairs were used as a negative control, to check autofluorescence signal occurrence and no signal were detected in the wavelengths range stated above.

RNA extraction and RT-qPCR. Total RNA was extracted using TRIZol (Invitrogen) and 2 µg were subjected to DNase treatment according to the manufacturer's protocol (Thermo Scientific). One µg of DNase-free RNA was reverse transcribed using Maxima H Minus Reverse Transcriptase (Thermo Scientific). RT-qPCR were performed using the LightCycler 480 SYBR Green I Master Kit on a LightCycler480 apparatus (Roche) using standard protocols (40 cycles, 60°C annealing). *PP2A* (AT1G13320; primers are listed in **Supplementary Table 3**) was used as reference.

RNA Immunoprecipitation. RNA immunoprecipitation (RIP) assays were performed on transiently transformed *N. benthamiana* leaves as described in (62), or in 10-day-old *A. thaliana 35S:WRKY42:GFP* seedlings as described in (63), using anti GFP (Abcam ab290) and anti-IgG (Abcam ab6702). RIP was performed using Invitrogen Protein A Dynabeads. Precipitated RNAs were prepared using TRI Reagent (Sigma-Aldrich), treated with DNase (Fermentas) and subjected to RT-qPCR (High Capacity cDNA Reverse Transcription Kit (Thermo); primers used are listed in **Supplementary Table 3**). Total RNAs were processed in parallel and considered the input sample.

Chromatin Immunoprecipitation. Chromatin immunoprecipitation (ChIP) assays were performed on 10-day-old WT seedlings treated or not during 24h at 10 °C, using anti H3K27me3 (Diagenode pAb-195-050), anti LHP1 (Covalab pab0923-P) and anti-IgG (Abcam ab6702), as described in (27). Crosslinked chromatin was sonicated using a water bath Bioruptor Pico (Diagenode; 30sec ON/30sec OFF pulses; 10 cycles; high intensity). ChIP was performed using Invitrogen Protein A Dynabeads. Precipitated DNA was recovered using Phenol:Chloroform:Isoamilic Acid (25:24:1; Sigma) and subjected to RT-qPCR (primers used are listed in **Supplementary Table 3**). Untreated sonicated chromatin was processed in parallel and considered the input sample. For *in vitro* competition assays, *APOLO* was transcribed using the T7 transcription kit (Promega; (27)). After regular chromatin isolation from 10-day-old *35S:WRKY42:GFP* seedlings, the sample was split in 4 independent tubes and diluted to 1ml in Nuclei Lysis Buffer without SDS. 0 µg, 0.1 µg, 1 µg and 10 µg of *APOLO* were added to each sample respectively, and incubated in rotation at 4 °C for 3h. Then, cross-linking was performed with 1% formaldehyde for 5 min at 4 °C, followed by 5 min with a final concentration of 50 mM glycine. SDS was added to a final concentration of 0.1% prior to sonication and the subsequent steps of a regular ChIP protocol.

Chromatin Isolation by RNA Purification followed by qPCR. A method adapted from the ChIRP protocol (64) was developed to allow the identification of plant DNA associated to specific lncRNAs, as described in (26, 27). Briefly, plants were *in vivo* crosslinked and cell nuclei were purified and extracted through sonication. The resulting supernatant was hybridized against biotinylated complementary oligonucleotides that tile the lncRNA of interest and lncRNA-associated chromatin was isolated using magnetic streptavidin beads. One hundred pmol of probes against *APOLO* (ODD and EVEN set of probes (26, 27)) and the corresponding negative set against LacZ were used for independent purification. Co-purified ribonucleoprotein complexes were eluted and used to purify RNA or DNA, which were later subjected to downstream assays for quantification as previously described (27).

Chromatin Conformation Capture. Chromosome conformation capture (3C) was performed basically as previously described in (27) starting with 2g of seedlings. Digestions were performed overnight at 37°C with 400U *Dpn*II (NEB). DNA was ligated by incubation at 16°C for 5h in 4 ml volume using 100U of T4 DNA ligase (NEB). After reverse crosslinking and Proteinase K treatment (Invitrogen), DNA was recovered by Phenol:Chloroform:Isoamilic Acid (25:24:1; Sigma) extraction and ethanol precipitation. Relative interaction frequency was calculated by qPCR (primers used are listed in **Supplementary Table 3**). A region free of *Dpn*II was used to normalize the amount of DNA.

Acknowledgments

We thank Chang Liu for providing the Hi-C plot of Figure 2B. This work was supported by grants from ANPCyT (PICT2016-0132 and PICT2017-0066) and Instituto Milenio iBio – Iniciativa Científica Milenio, MINECON to JME; ANPCyT (PICT2016-0007 and PICT2016-0289) to FA; UNL (CAI+D 2016) to LL; Laboratoire d'Excellence (LABEX) Saclay Plant Sciences (SPS; ANR-10-LABX-40) to MC; and CNRS (Laboratoire International Associé NOCOSYM) to MC and FA. LL, FI, JME and FA are researchers of CONICET; MM, JMP, CFF and JRM are fellows of the same institution.

Author contributions

MM, JMP, LL, CFF, JRM, AC, MB and FA performed the experiments. JB, MB, FI, MC, JE and FA analyzed the data. JE and FA conceived the project. FA, JE and CFF wrote the manuscript with the contribution of all authors.

References

1. K. H. Ryu, *et al.*, The WEREWOLF MYB protein directly regulates CAPRICE transcription during cell fate specification in the Arabidopsis root epidermis. *Development* **132**, 4765–4775 (2005).
2. S. K. Song, *et al.*, Cell fate in the Arabidopsis root epidermis is determined by competition between WEREWOLF and CAPRICE. *Plant Physiol.* **157**, 1196–1208 (2011).
3. J. Schiefelbein, L. Huang, X. Zheng, Regulation of epidermal cell fate in Arabidopsis roots: The importance of multiple feedback loops. *Front. Plant Sci.* **5** (2014).
4. D. Balcerowicz, S. Schoenaers, K. Vissenberg, Cell fate determination and the switch from diffuse growth to planar polarity in arabidopsis root epidermal cells. *Front. Plant Sci.* **6**, 1163 (2015).
5. Q. Lin, *et al.*, GLABRA2 directly suppresses basic helix-loop-helix transcription factor genes with

diverse functions in root hair development. *Plant Cell* **27**, 2894–2906 (2015).

6. B. Menand, *et al.*, An ancient mechanism controls the development of cells with a rooting function in land plants. *Science (80-.).* **316**, 1477–1480 (2007).

7. N. D. Pires, *et al.*, Recruitment and remodeling of an ancient gene regulatory network during land plant evolution. *Proc. Natl. Acad. Sci. U. S. A.* **110**, 9571–9576 (2013).

8. B. Karas, *et al.*, Conservation of Lotus and Arabidopsis basic helix-loop-helix proteins reveals new players in root hair development. *Plant Physiol.* **151**, 1175–1185 (2009).

9. K. Yi, B. Menand, E. Bell, L. Dolan, A basic helix-loop-helix transcription factor controls cell growth and size in root hairs. *Nat. Genet.* **42**, 264–267 (2010).

10. A. Bruex, *et al.*, A gene regulatory network for root epidermis cell differentiation in Arabidopsis. *PLoS Genet.* **8** (2012).

11. S. K. Won, *et al.*, cis-element- and transcriptome-based screening of root hair-specific genes and their functional characterization in Arabidopsis. *Plant Physiol.* **150**, 1459–1473 (2009).

12. S. Datta, H. Prescott, L. Dolan, Intensity of a pulse of RSL4 transcription factor synthesis determines Arabidopsis root hair cell size. *Nat. Plants* **1**, 1–6 (2015).

13. P. Vijayakumar, S. Datta, L. Dolan, ROOT HAIR DEFECTIVE SIX-LIKE4 (RSL4) promotes root hair elongation by transcriptionally regulating the expression of genes required for cell growth. *New Phytol.* **212**, 944–953 (2016).

14. C. Ringli, The hydroxyproline-rich glycoprotein domain of the Arabidopsis LRX1 requires Tyr for function but not for insolubilization in the cell wall. *Plant J.* **63**, 662–669 (2010).

15. S. M. Velasquez, *et al.*, O-glycosylated cell wall proteins are essential in root hair growth. *Science (80-.).* **332**, 1401–1403 (2011).

16. Y. Hwang, H. S. Choi, H. M. Cho, H. T. Cho, Tracheophytes contain conserved orthologs of a basic helix-loop-helix transcription factor that modulate ROOT HAIR SPECIFIC genes. *Plant Cell* **29**, 39–53 (2017).

17. S. Mangano, *et al.*, Molecular link between auxin and ROS-mediated polar growth. *Proc. Natl. Acad. Sci. U. S. A.* **114**, 5289–5294 (2017).

18. R. Bhosale, *et al.*, A mechanistic framework for auxin dependent Arabidopsis root hair elongation to low external phosphate. *Nat. Commun.* **9** (2018).

19. E. Marzol, C. Borassi, S. P. Denita Juárez, S. Mangano, J. M. Estevez, RSL4 Takes Control: Multiple Signals, One Transcription Factor. *Trends Plant Sci.* **22**, 553–555 (2017).

20. B. N. Devaiah, A. S. Karthikeyan, K. G. Raghothama, WRKY75 transcription factor is a modulator of

460 phosphate acquisition and root development in Arabidopsis. *Plant Physiol.* **143**, 1789–1801
461 (2007).
462 21. Y. F. Chen, *et al.*, The WRKY6 transcription factor modulates PHOSPHATE1 expression in response
463 to low pi stress in arabidopsis. *Plant Cell* **21**, 3554–3566 (2009).
464 22. H. Wang, *et al.*, Arabidopsis WRKY45 transcription factor activates Phosphate transporter1;1 ex-
465 pression in response to phosphate starvation. *Plant Physiol.* **164**, 2020–2029 (2014).
466 23. T. Su, *et al.*, WRKY42 Modulates phosphate homeostasis through regulating phosphate translocа-
467 tion and acquisition in Arabidopsis. *Plant Physiol.* **167**, 1579–1591 (2015).
468 24. J. M. Franco-Zorrilla, *et al.*, Target mimicry provides a new mechanism for regulation of microRNA
469 activity. *Nat. Genet.* **39**, 1033–1037 (2007).
470 25. M. Jabnoune, *et al.*, A Rice cis-Natural antisense RNA acts as a translational enhancer for its cog-
471 nate mRNA and contributes to phosphate homeostasis and plant fitness. *Plant Cell* **25**, 4166–4182
472 (2013).
473 26. F. Ariel, *et al.*, Noncoding transcription by alternative rna polymerases dynamically regulates an
474 auxin-driven chromatin loop. *Mol. Cell* **55**, 383–396 (2014).
475 27. F. Ariel, *et al.*, R-Loop Mediated trans Action of the APOLO Long Noncoding RNA. *Mol. Cell* **77**,
476 1055-1065.e4 (2020).
477 28. D. T. A. Lamport, M. J. Kieliszewski, Y. Chen, M. C. Cannon, Role of the Extensin Superfamily in
478 Primary Cell Wall Architecture. *Plant Physiol.* **156**, 11–19 (2011).
479 29. S. M. Velasquez, *et al.*, Low sugar is not always good: Impact of specific o-glycan defects on tip
480 growth in arabidopsis. *Plant Physiol.* **168**, 808–813 (2015).
481 30. E. Marzol, *et al.*, Filling the Gaps to Solve the Extensin Puzzle. *Mol. Plant* **11**, 645–658 (2018).
482 31. T.Q. Zhang, Z.G. Xu, G.D. Shang, J.W. Wang, A Single-Cell RNA Sequencing Profiles the Develop-
483 mental Landscape of Arabidopsis Root. *Mol Plant*. 12, 648-660 (2019).
484 32. P. Gyula, *et al.*, Ambient temperature regulates the expression of a small set of sRNAs influencing
485 plant development through NF-YA2 and YUC2. *Plant Cell Environ.* **41**, 2404–2417 (2018).
486 33. A. Veluchamy, *et al.*, LHP1 Regulates H3K27me3 Spreading and Shapes the Three-Dimensional
487 Conformation of the Arabidopsis Genome. *PLoS One* **11**, e0158936 (2016).
488 34. W. Xu, *et al.*, The R-loop is a common chromatin feature of the Arabidopsis genome. *Nat. Plants*
489 **3**, 704–714 (2017).
490 35. C. Liu, *et al.*, Genome-wide analysis of chromatin packing in Arabidopsis thaliana at single-gene
491 resolution. *Genome Res.* **26**, 1057–1068 (2016).

36. M. Ikeuchi, *et al.*, PRC2 represses dedifferentiation of mature somatic cells in Arabidopsis. *Nat. Plants* **1**, 1–7 (2015).

37. J. Waese, *et al.*, ePlant: Visualizing and Exploring Multiple Levels of Data for Hypothesis Generation in Plant Biology. *Plant Cell* **29**, 1806-1821 (2017).

38. H. Jiang, *et al.*, Long non-coding RNA SNHG15 interacts with and stabilizes transcription factor Slug and promotes colon cancer progression. *Cancer Lett.* **425**, 78–87 (2018).

39. T. Hung, *et al.*, Extensive and coordinated transcription of noncoding RNAs within cell-cycle promoters in *Nature Genetics*, (NIH Public Access, 2011), pp. 621–629.

40. I. Martianov, *et al*., Repression of the human dihydrofolate reductase gene by a non-coding interfering transcript. *Nature* **445**, 666-670 (2007).

41. A. N. Stepanova, *et al*., TAA1-Mediated Auxin Biosynthesis Is Essential for Hormone Crosstalk and Plant Development. *Cell* **133**, 177–191 (2008).

42. A. R. Jones, *et al.*, Auxin transport through non-hair cells sustains root-hair development. *Nat. Cell Biol.* **11**, 78–84 (2009).

43. Q. Wang, *et al.*, A phosphorylation-based switch controls TAA1-mediated auxin biosynthesis in plants. *Nat. Commun.* **11**, 679 (2020).

44. S. Mangano, S. P. Denita-Juarez, E. Marzol, C. Borassi, J. M. Estevez, High auxin and high phosphate impact on rsl2 expression and ros-homeostasis linked to root hair growth in Arabidopsis thaliana. *Front. Plant Sci.* **9** (2018).

45. S. Schoenaers, *et al.*, The Auxin-Regulated CrRLK1L Kinase ERULUS Controls Cell Wall Composition during Root Hair Tip Growth. *Curr. Biol.* **28**, 722-732.e6 (2018).

46. J. Friml, *et al.*, A PINOID-dependent binary switch in apical-basal PIN polar targeting directs auxin efflux. *Science (80-.).* **306**, 862–865 (2004).

47. S. Mangano, J. Martínez Pacheco, C. Marino-Buslje, J. M. Estevez, How Does pH Fit in with Oscillating Polar Growth? *Trends Plant Sci.* **23**, 479–489 (2018).

48. S. Guimil, C. Dunand, Patterning of Arabidopsis epidermal cells: epigenetic factors regulate the complex epidermal cell fate pathway. *Trends Plant Sci.* **11**, 601–609 (2006).

49. S. Costa, P. Shaw, Chromatin organization and cell fate switch respond to positional information in Arabidopsis. *Nature* **439**, 493–496 (2006).

50. C. C. Beyrne, N. D. Iusem, R. M. González, Effect of salt stress on cytosine methylation within GL2,

an Arabidopsis thaliana gene involved in root epidermal cell differentiation. Absence of inheritance in the unstressed progeny. *Int. J. Mol. Sci.* **20** (2019).

51 L. Lucero, *et al.*, Long noncoding RNAs shape transcription in plants. *Transcription* (2020).

52. S. Marquardt, *et al.*, Functional Consequences of Splicing of the Antisense Transcript COOLAIR on FLC Transcription. *Mol. Cell* **54**, 156–165 (2014).

53. F. Liu, S. Marquardt, C. Lister, S. Swiezewski, C. Dean, Targeted 3' processing of antisense transcripts triggers arabidopsis FLC chromatin silencing. *Science (80-.).* **327**, 94–97 (2010).

54. J. B. Heo, S. Sung, Vernalization-mediated epigenetic silencing by a long intronic noncoding RNA. *Science (80-.).* **331**, 76–79 (2011).

55. D. H. Kim, S. Sung, Vernalization-Triggered Intragenic Chromatin Loop Formation by Long Noncoding RNAs. *Dev. Cell* **40**, 302-312.e4 (2017).

56. P. Kindgren, R. Ard, M. Ivanov, S. Marquardt, Transcriptional read-through of the long non-coding RNA SVALKA governs plant cold acclimation. *Nat. Commun.* **9**, 1–11 (2018).

57. F. Ariel, *et al.*, Battles and hijacks: noncoding transcription in plants. *TiPS* **20**, 362–371 (2015).

58. Y. Kotake, *et al.*, Long Non-coding RNA, PANDA, Contributes to the Stabilization of p53 Tumor Suppressor Protein. *Anticancer Res.* **36**, 1605–11 (2016).

59. W. Shi, *et al.*, Long noncoding RNA PANDA promotes esophageal squamous carcinoma cell progress by dissociating from NF-YA but interact with SAFA. *Pathol. Research and Practice* **215**, 152604 (2019).

60. P. K. Puvvula, *et al.*, Long noncoding RNA PANDA and scaffold-attachment-factor SAFA control senescence entry and exit. *Nat. Commun.* **5** (2014).

61. S.J. Clough, A.F. Bent, Floral dip: a simplified method for Agrobacterium -mediated transformation of Arabidopsis thaliana. *The Plant Journal* **16**, 735-743 (1998).

62. R. Sorenson, J. Bailey-Serres, Rapid immunopurification of ribonucleoprotein complexes of plants. *Methods Mol. Biol.* **1284**, 209–219 (2015).

63. F. Bardou, *et al.*, Long Noncoding RNA Modulates Alternative Splicing Regulators in Arabidopsis. *Dev. Cell* **30**, 166–176 (2014).

64. C. Chu, J. Quinn, H. Y. Chang, Chromatin isolation by RNA purification (ChIRP). *J. Vis. Exp.* (2012) https:/doi.org/10.3791/3912.

65. J. Dong, C. Chen, Z. Chen, Expression profiles of the Arabidopsis WRKY gene superfamily during plant defense response. *Plant Mol. Biol.* **51**, 21–37 (2003).

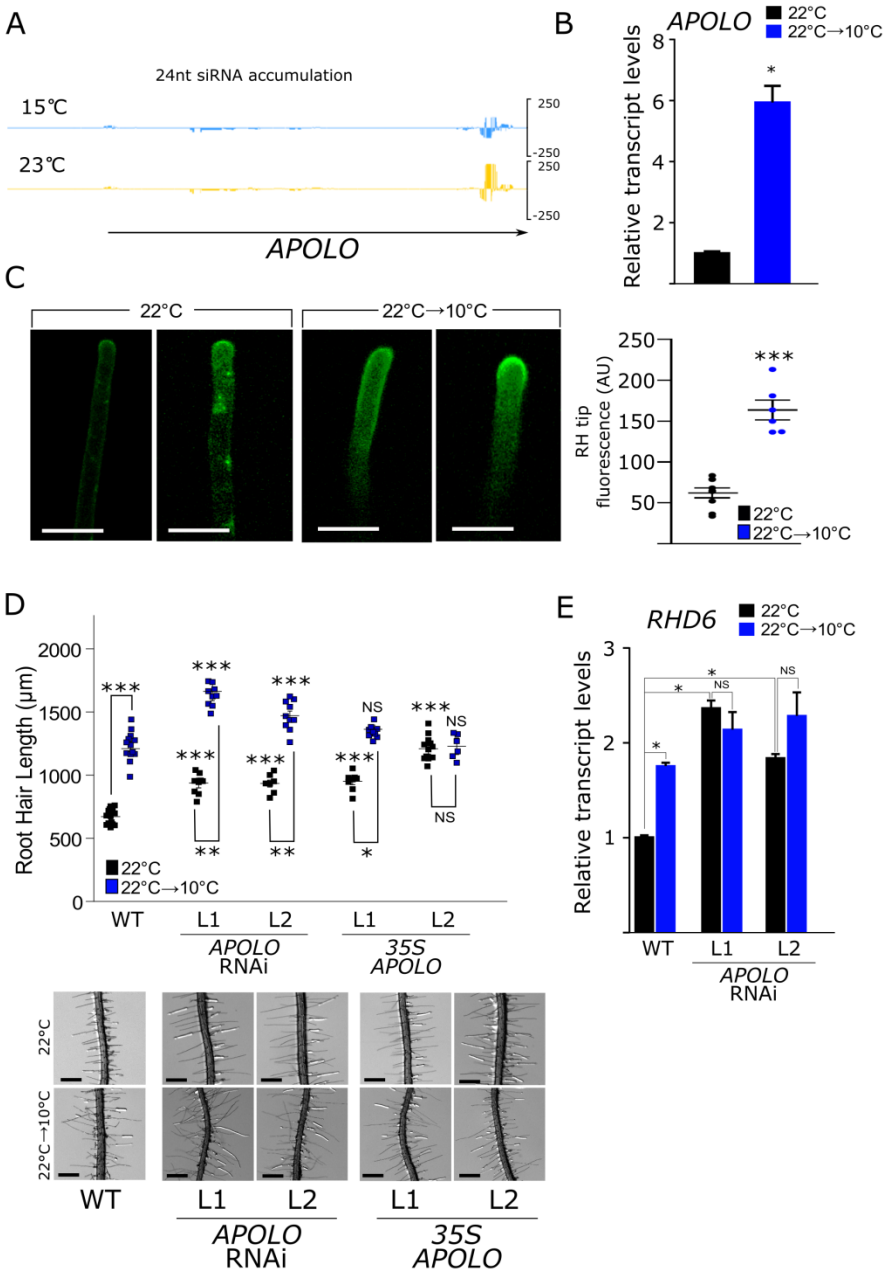

Figure 1. *APOLO* regulates root hair elongation in response to low temperatures

A. 24nt siRNA accumulation over the *APOLO* locus revealed by small RNA-Seq of roots from WT seedlings grown at 15 °C or 23 °C (32).

B. *APOLO* transcript levels measured by RT-qPCR in roots of 10-day-old plants grown at 22 °C treated or not for 24h at 10 °C.

C. The *APOLO* promoter region (full intergenic region between *PID* and *APOLO*) is active in root hairs at 22 °C and 10 °C, using the *GFP* reporter gene. Images are representative of the lowest and highest GFP signal detected in the observation of several roots. The quantification of the fluorescence is shown in the right panel.

D. Quantification of RH length of 8-day-old WT, RNAi-*APOLO* and *35S:APOLO* plants, respectively, at 22 °C and 10 °C. Each point is the mean of the length of the 10 longest RHs identified in a single root. Repre-

sentative images of each genotype are shown below the graph. Asterisks indicate significant differences between WT and the corresponding genotype at the same temperature (one way ANOVA followed by a Tukey-Kramer test; "*"<0.05, "**"<0.01, "***"<0.001, NS: no statistically significant).

E. *RHD6* transcript levels measured by RT-qPCR in roots of WT plants vs. two independent RNAi-*APOLO* lines grown at 22 °C treated or not for 24h at 10 °C.

In B and E, the error bar represents the SD of 3 biological replicates. The asterisk indicates that the difference is significant (t test p<0.05).

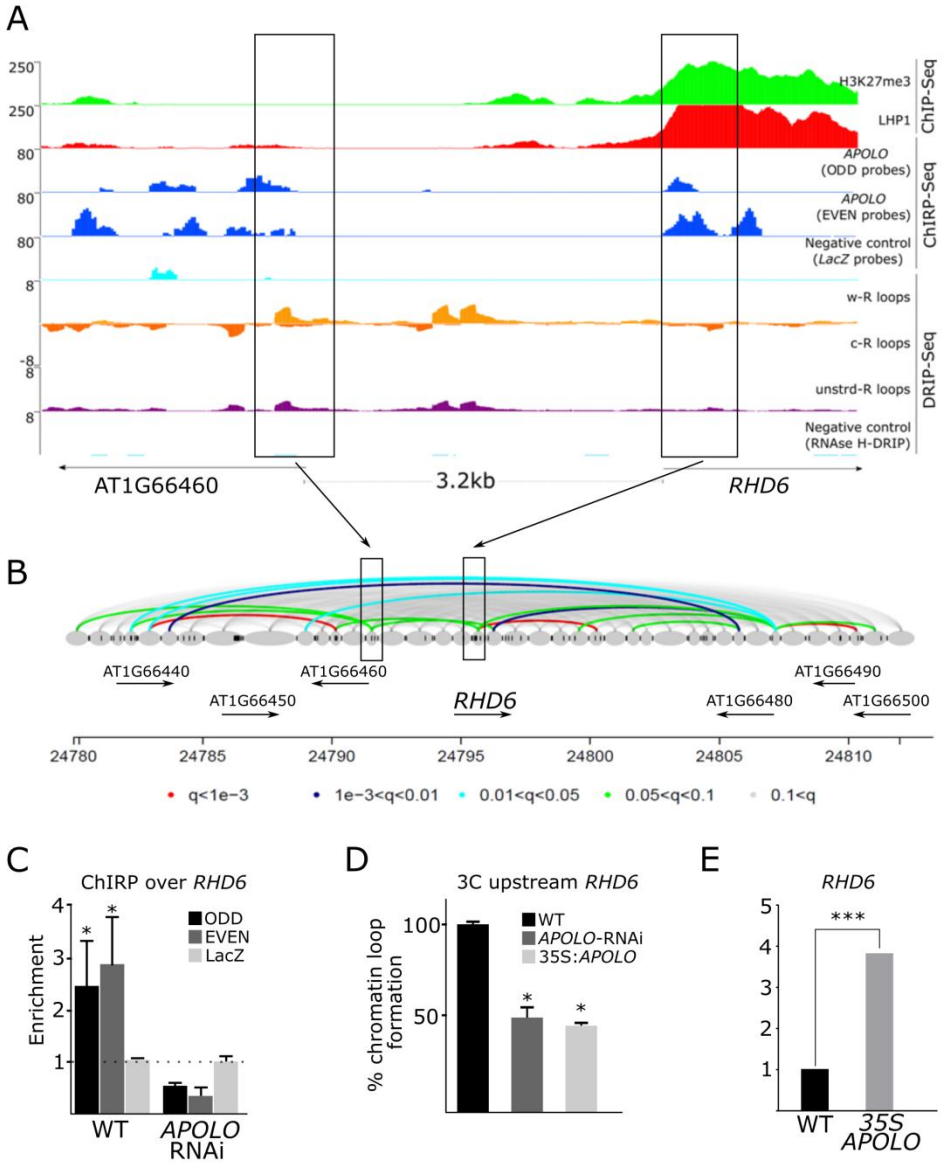

Figure 2. *APOLO* directly modulates chromatin three-dimensional conformation of the *RHD6* locus

A. Epigenomic landscape of the *RHD6* locus. Lane 1: H3K27me3 deposition by ChIP-Seq (33). Lane 2: LHP1 deposition by ChIP-Seq (33). Lane 3 to 5: *APOLO* recognition by ChIRP-Seq (Lane 3 and 4, using ODD and EVEN sets of probes against *APOLO*, respectively; Lane 5, negative control using LacZ probes)(27). Lane 6 to 9: R-loop formation by DRIP-Seq (34), on Watson strand (Lane 6), Crick strand (Lane 7) or unstranded sequencing (Lane 8). DRIP negative control after RNAseH treatment is shown in Lane 9. Gene annotation is shown at the bottom.

B. Chromatin loops identified in the *RHD6* region by *Dpn*II HiC (35). Colors of the loops are related to the corresponding q-values indicated below. Black boxes in A and B indicate the same genomic locations, where the bases of the chromatin loop correlate with R-loop formation and *APOLO* recognition (compared to gene annotations).

C. *APOLO* association to DNA of the *RHD6* locus by ChIRP-qPCR in WT and RNAi-*APOLO* plants. The background level was determined using a set of probes against LacZ RNA.

588 **D.** Relative chromatin loop formation by 3C-qPCR deduced from **B**, in WT plants vs. *35S:APOLO* and RNAi
589 lines for the region upstream *RHD6*.
590 **E.** *RHD6* transcript levels revealed by RNA-Seq of WT vs. *35S:APOLO* plants(27).
591 In C and D, the error bar represents the SD of 3 biological replicates. The asterisk indicates that the dif-
592 ference is significant (t test "*"<0.05). In E, p-value from RNA-Seq (27) "***"<0.001.
593

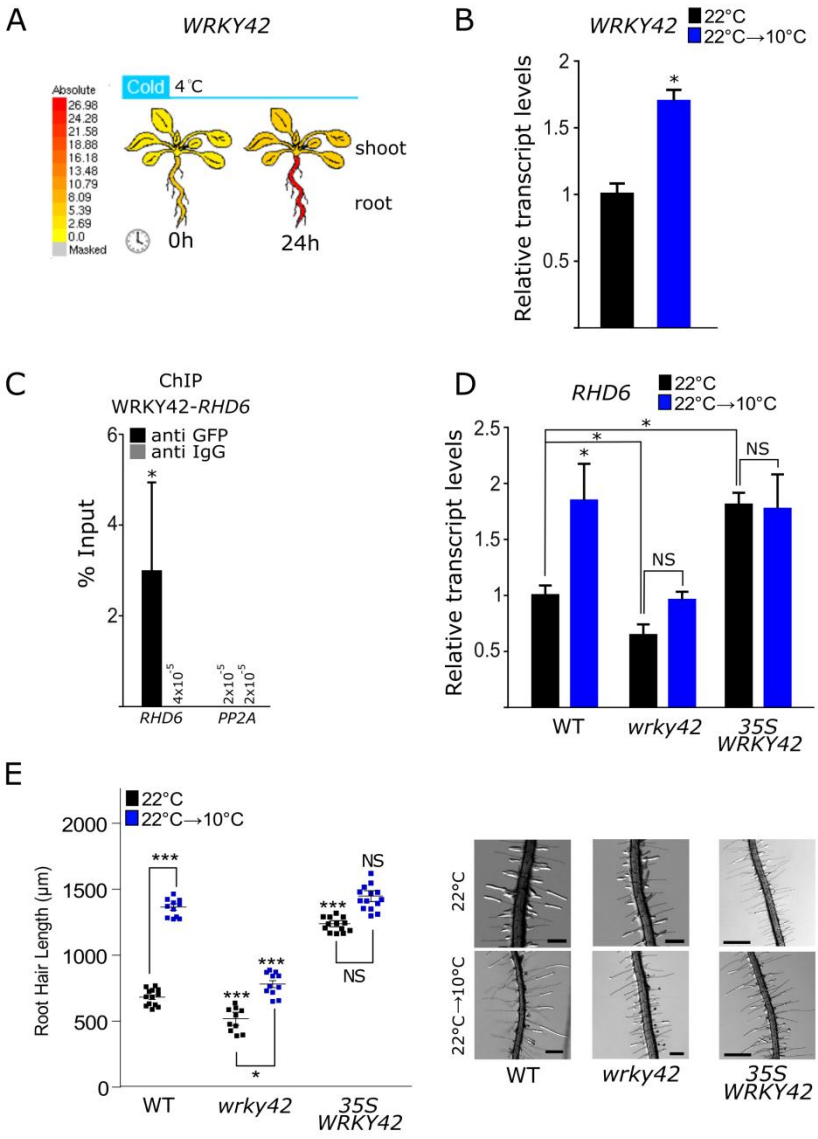

Figure 3. The transcription factor WRKY42 directly regulates *RHD6* and participates in the response to cold

A. Arabidopsis eFP Browser (37) plot representing the increase of *WRKY42* transcript levels in roots of seedlings treated for 24h at 4°C.

B. *WRKY42* transcript levels measured by RT-qPCR in roots of plants grown at 22°C treated or not for 24h at 10°C.

C. Chromatin Immunoprecipitation (ChIP)-qPCR assay revealing regulation by WRKY42 of *RHD6* by direct recognition of its promoter region. Probes amplifying *PP2A* were used as a negative control of the experiment. Anti-IgG antibodies were used as a negative control for each pair of probes.

D. *RHD6* transcript levels measured by RT-qPCR in roots of WT plants vs. *wrky42* mutants and *35S:WRKY42:GFP* lines grown at 22°C treated or not for 24h at 10°C.

E. Quantification of RH length of plants WT, *wrky42* and *35S:WRKY42:GFP* at 22°C and 10°C. Each point is the mean of the length of the 10 longest RHs identified in a single root. Representative images of each

609 genotype are shown on the right. Asterisks indicate significant differences between WT and the corre-
610 sponding genotype at the same temperature (one way ANOVA followed by a Tukey-Kramer test;
611 “*”<0.05, “***”<0.001, NS: no statistically significant).
612 In B, C and D, the error bar represents the SD of 3 biological replicates. The asterisk indicates that the
613 difference is significant (t test p<0.05, NS: no statistically significant).
614

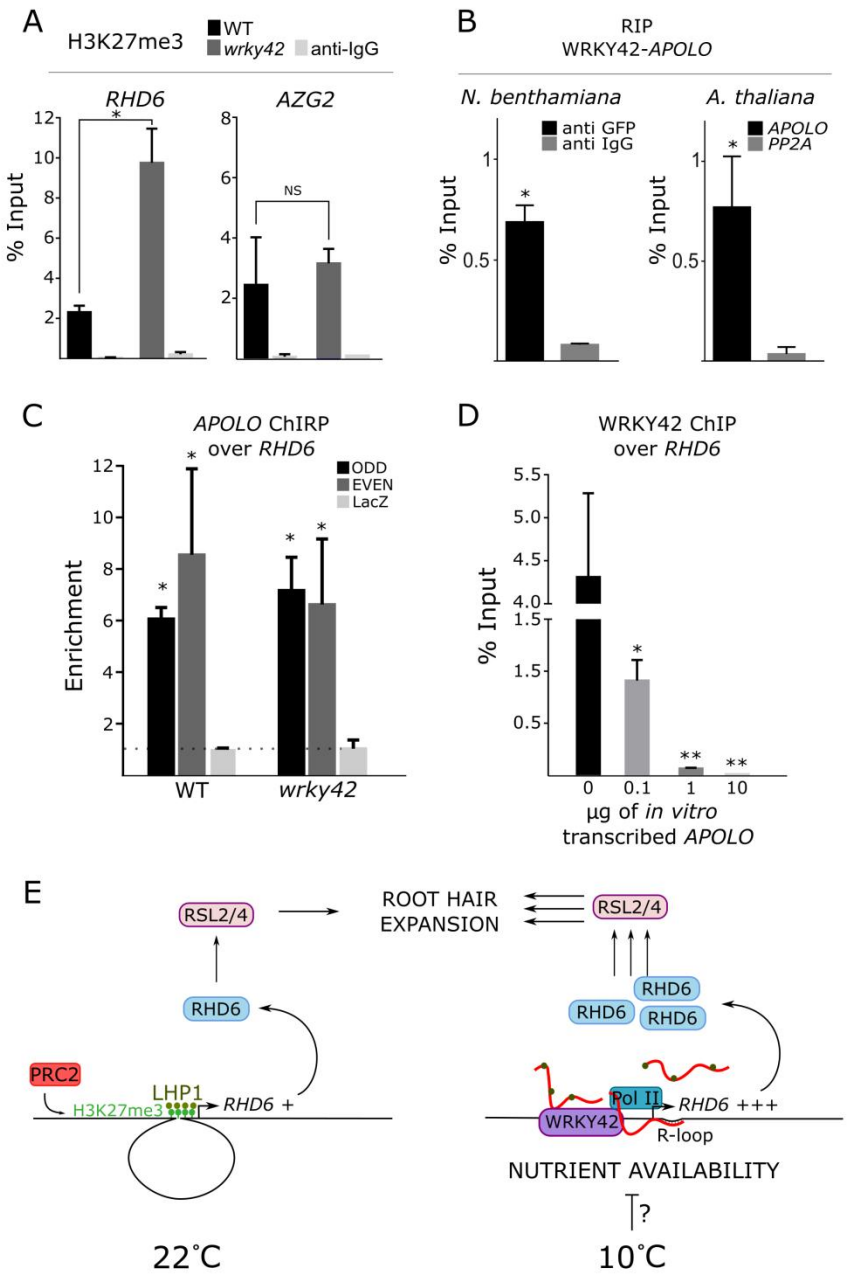

615

616 **Figure 4. The WRKY42-*APOLO* hub activates *RHD6* transcription in response to low temperatures, pro-**
617 **moting root hair expansion**

618 **A.** H3K27me3 deposition in WT vs. *wrky42* mutant 10-day-old seedlings grown at 23°C over *RHD6* and a
619 WRKY42-independent *APOLO* target (*AZG2*; (27)). An immunoprecipitation (ChIP-qPCR) was performed
620 using an anti-IgG antibody as a negative control.

621 **B.** *APOLO*-WRKY42 interaction *in vivo* demonstrated by RNA Immunoprecipitation (RIP)-qPCR in transi-
622 ently transformed tobacco leaves and stably transformed Arabidopsis plants. In tobacco, WRKY42:GFP
623 and *APOLO* were co-transformed under the control of the 35S constitutive promoter. In Arabidopsis,
624 *35S:WRKY42:GFP* transformed plants were used to detect the interaction with endogenous *APOLO*. Anti-

IgG antibodies were used as a negative control. The RNA *PP2A* was considered as a RIP negative control in Arabidopsis plants.

C. *APOLO* association to DNA of the *RHD6* locus by ChIRP-qPCR in WT and *wrky42* mutant plants. The background level was determined using a set of probes against LacZ RNA.

D. WRKY42 immunoprecipitation over *RHD6* with the addition of increasing concentrations of *in vitro* transcribed *APOLO* prior to cross-linking.

E. Proposed model for the action of *APOLO* in RH growth under low temperatures. In response to cold, *APOLO* levels increase, recognizing the *RHD6* locus by sequence complementarity. Then, LHP1 is decoyed away from chromatin and H3K27me3 deposition decreases in a process involving WRKY42 and leading to the opening of the *RHD6* promoter region. Additionally, *APOLO* and WRKY42 jointly activate *RHD6* transcription. RHD6 activates the transcription of downstream TF genes *RSL2* and *4* promoting RH cell expansion.

In A, B, C and D, the error bar represents the SD of 3 biological replicates. The asterisk indicates that the difference is significant (t test "*"<0.05, "**"<0.01).

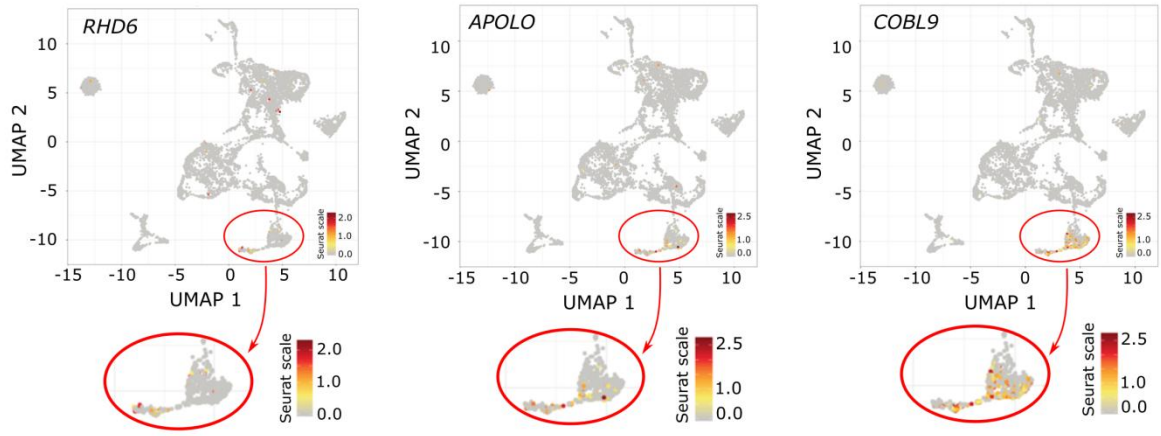

Supplementary Figure 1: *RHD6* and *APOLO* transcripts are enriched in root hair cells

Uniform Manifold Approximation and Projection (UMAP) clustering map of Arabidopsis root single cell RNA-seq ((31; http://wanglab.sippe.ac.cn/rootatlas/) data. *RHD6*, *APOLO* and the trichoblast cell marker *COBL9* are respectively indicated in red in each plot.

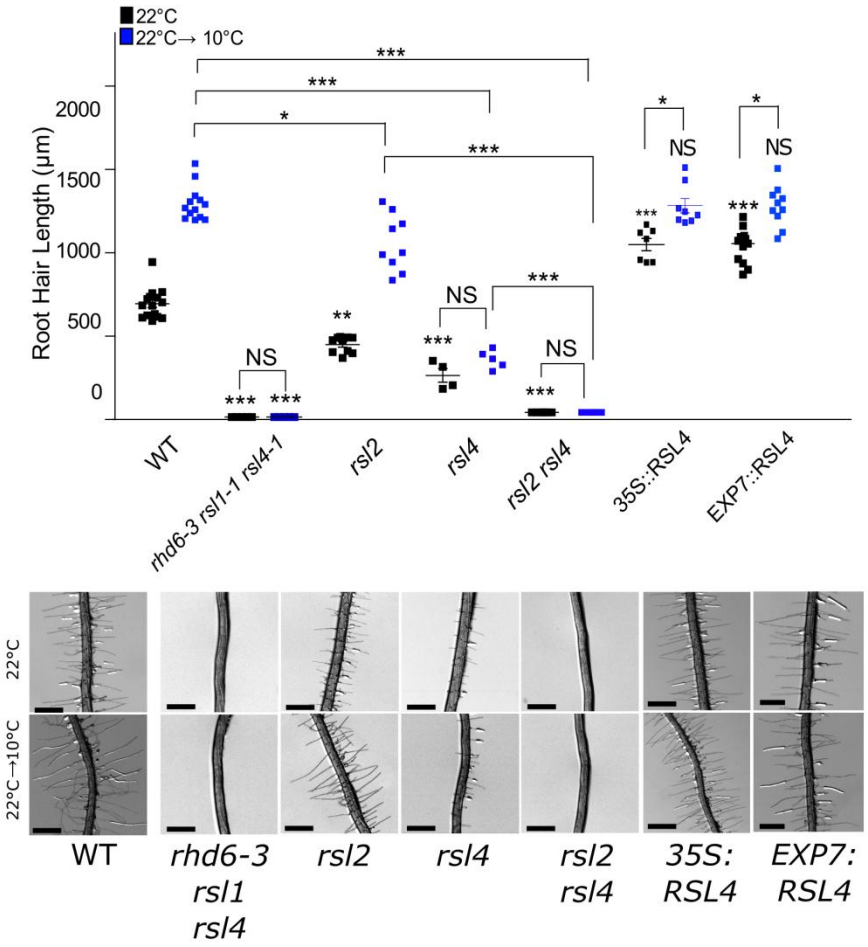

Supplementary Figure 2. Root hair expansion in response to cold is mediated by *RSL2* and *RSL4*

Quantification of RH length of plants WT, *rhd6-3, rsl1/4; rsl2; rsl4; rsl2/4*; *35S:RSL4* and *pEXP7:RSL4* at 22°C and 10°C. Each point is the mean of the length of the 10 longest RHs identified in a single root. Representative images of each genotype are shown below the graph. Asterisks indicate significant differences between WT and the corresponding genotype at the same temperature (one way ANOVA followed by a Tukey-Kramer test; "*"<0.05, "**"<0.01, "***"<0.001, NS: no statistically significant), unless indicated differently.

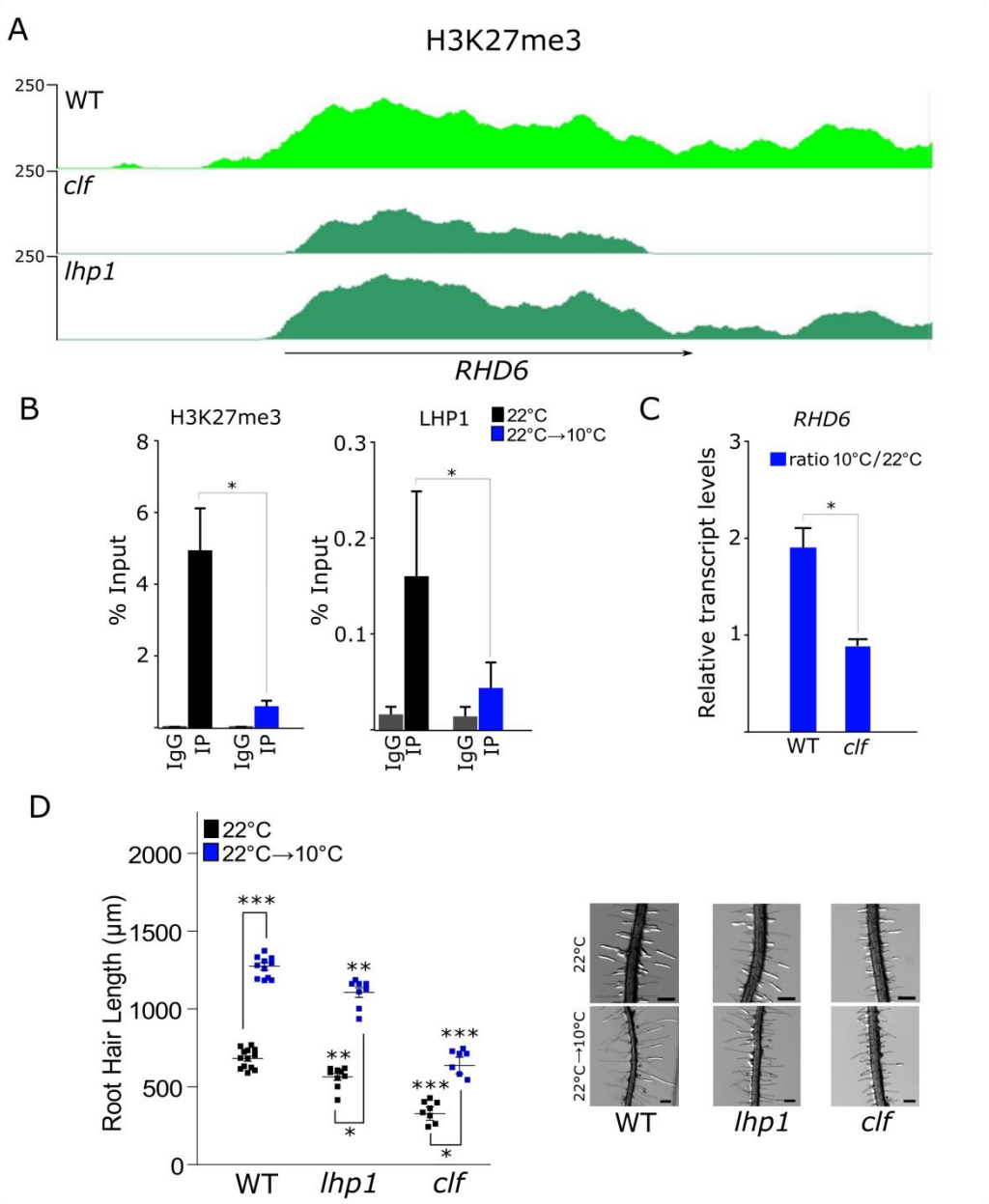

Supplementary Figure 3: Induction of root hair elongation by low temperatures requires epigenetic Polycomb-mediated reprogramming

A. H3K27me3 deposition across the *RHD6* locus in WT, *clf* and *lhp1* mutants, revealed by ChIP-seq from seedlings grown at 23°C (33).

B. H3K27me3 deposition measured by ChIP-qPCR over the *RHD6* locus in WT plants grown at 22°C treated or not for 24h at 10°C. The negative control was performed using an anti-IgG antibody.

C. *RHD6* transcript levels measured by RT-qPCR in roots of WT plants vs. *clf* mutants, expressed as the ratio between plants treated or not for 24h at 10°C over the mock plants grown at 22°C.

D. Quantification of RH length of plants WT, *lhp1* and *clf* at 22°C and 10°C. Each point is the mean of the length of the 10 longest RHs identified in a single root. Representative images of each genotype are shown on the right. Asterisks indicate significant differences between WT and the corresponding geno-

667 type at the same temperature (one way ANOVA followed by a Tukey-Kramer test; "**"<0.01,
668 "***"<0.001).
669 In B and C, the error bar represents the SD of 3 biological replicates. The asterisk indicates that the dif-
670 ference is significant (t test p<0.05).

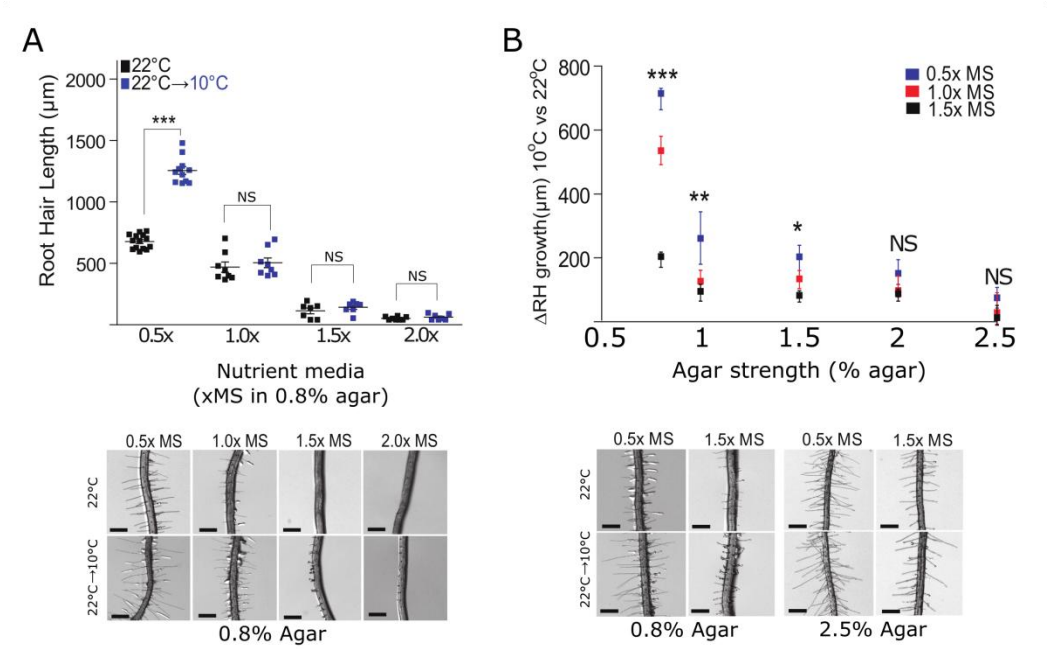

Supplementary Figure 4. Root hair expansion in response to cold seems to be related to nutrient availability

A. Quantification of RH length of WT plants at 22°C and 10°C at growing concentrations of Murashige and Skoog (MS) culture media. Each point is the mean of the length of the 10 longest RHs identified in a single root. Representative images of each genotype are shown on the right. Asterisks indicate significant differences between WT cultivated in the same growth conditions at different temperatures (one way ANOVA followed by a Tukey-Kramer test). NS stands for no statistically significant difference.

B. Quantification of RH length of WT plants expressed as the ratio between 10°C and 22°C at growing concentrations of MS culture media, for given concentrations of agar. Each point is the mean of the length of the 10 longest RHs identified in a single root. Representative images of each genotype are shown below the graph.

Asterisks indicate significant differences between the ratio of WT cultivated at different temperatures in different growth conditions (one way ANOVA followed by a Tukey-Kramer test; "*"<0.05, "**"<0.01, "***"<0.001, NS: no statistically significant).

686 **LEGENDS TO SUPPLEMENTARY TABLES**
687
688 **Supplementary Table 1: *APOLO* targets related to root hair growth**
689 The list of *APOLO bona fide* targets was determined in (27). The search for root hairs-related genes was
690 performed based on (9, 11, 13, 16). LHP1 binding and H3K27me3 deposition was investigated in previ-
691 ously published datasets (33). W-boxes (TTGACY; (65)) present in the first 2500 bp upstream the ATG of
692 each gene was searched manually. The position of the W-box is given only for *RHD6*, directly recognized
693 by WRKY42 (**Figure 4B**).
694
695 **Supplementary Table 2: Root hair-related genes deregulated in *35S:APOLO* seedlings**
696 The list of deregulated genes was determined by RNA-Seq (27). The search for root hairs-related genes
697 was performed based on (9, 11, 13, 16). Genes are classified as directly (same as in **Supplementary Table**
698 **1**) or indirectly regulated by *APOLO*. *RHD6*, *RSL2* and *RSL4* are highlighted in red.
699
700 **Supplementary Table 3: List of oligonucleotides used in this work**

Supplementary Table 1

APOLO target	Gene name	LHP1 binding	H3K27me3 deposition	W-boxes in promoter	WRKY42 target (position)
AT1G66470	*RHD6*	YES	YES	1	-2521
AT1G21310	*EXT3*	YES	YES	4	
AT1G23720	*EXT15*	YES	YES	3	
AT1G26250	*EXT18*	YES	YES	0	
AT1G62440	*LRX2*	YES	YES	1	
AT2G04780	*FLA7*	NO	NO	2	
AT2G24980	*EXT6*	weak	weak	2	
AT2G26420	*PIP5K3*	NO	NO	2	
AT3G14310	*PME3*	NO	NO	0	
AT3G54580	*EXT17*	weak	NO	1	
AT4G08400	*EXT7*	weak	NO	2	
AT4G08410	*EXT8*	weak	NO	0	
AT4G13340	*LRX3*	weak	NO	3	
AT4G13390	*EXT12*	weak	weak	0	
AT4G40090	*AGP3*	YES	YES	2	
AT5G06630	*EXT9*	YES	YES	1	
AT5G06640	*EXT10*	YES	YES	0	

Supplementary Table 2

	gene	name	locus	sample 1	sample 2	status	value 1	value 2	log2(FC)	test stat	p value	q value	significant?
APOLO **direct** targets (Supplementary Table 1)	AT1G66470	***RHD6***	chr1:24795213-24796988	WT	*35S:APOLO*	OK	0,376783	1,05922	1,4912	2,64116	0,00015	0,00097	yes
	AT1G21310	***EXT3***	chr1:7453235-7455069	WT	*35S:APOLO*	OK	152,749	461,038	1,59372	6,83739	5,00E-05	0,00035	yes
	AT1G23720	***EXT15***	chr1:8388654-8391540	WT	*35S:APOLO*	OK	3,09641	19,245	2,63582	10,0477	0,00005	0,00035	yes
	AT1G26250	***EXT18***	chr1:9083837-9085464	WT	*35S:APOLO*	OK	3,22367	1,51056	-1,09362	-2,90259	0,00005	0,00035	yes
	AT1G62440	***LRX2***	chr1:23111817-23115508	WT	*35S:APOLO*	OK	0,292088	2,59795	3,1529	6,79781	5,00E-05	0,00035	yes
	AT2G04780	***FLA7***	chr2:1676741-1678455	WT	*35S:APOLO*	OK	7,18037	16,6557	1,21388	4,52231	0,00005	0,00035	yes
	AT2G24980	***EXT6***	chr2:10622452-10624132	WT	*35S:APOLO*	OK	0,837653	6,96907	3,05654	7,82993	5,00E-05	0,00035	yes
	AT2G26420	***PIP5K3***	chr2:11239433-11242239	WT	*35S:APOLO*	OK	0,077305	0,34491	2,15759	2,67767	0,0003	0,00181	yes
	AT3G14310	***PME3***	chr3:4771901-4775119	WT	*35S:APOLO*	OK	12,0768	25,3357	1,06894	4,63885	0,00005	0,00035	yes
	AT3G54580	***EXT17***	chr3:20200687-20203782	WT	*35S:APOLO*	OK	2,80301	22,185	2,98453	11,514	5,00E-05	0,00035	yes
	AT4G08400	***EXT7***	chr4:5323799-5325341	WT	*35S:APOLO*	OK	0,166086	2,09646	3,65795	5,75847	5,00E-05	0,00035	yes
	AT4G08410	***EXT8***	chr4:5339085-5341209	WT	*35S:APOLO*	OK	0,242031	2,59029	3,41985	6,63579	5,00E-05	0,00035	yes
	AT4G13340	***LRX3***	chr4:7758609-7761159	WT	*35S:APOLO*	OK	61,2495	139,492	1,18741	5,4	5,00E-05	0,00035	yes
	AT4G13390	***EXT12***	chr4:7783802-7785332	WT	*35S:APOLO*	OK	1,28902	9,4516	2,87429	7,90266	5,00E-05	0,00035	yes
	AT4G40090	***AGP3***	chr4:18580837-18581585	WT	*35S:APOLO*	OK	0,465013	6,11837	3,71781	6,1024	0,00005	0,00035	yes
	AT5G06630	***EXT9***	chr5:2036360-2037843	WT	*35S:APOLO*	OK	0,47843	4,28202	3,16191	6,69628	5,00E-05	0,00035	yes
	AT5G06640	***EXT10***	chr5:2039858-2041928	WT	*35S:APOLO*	OK	0,704936	6,53659	3,21297	8,39508	5,00E-05	0,00035	yes
RH-related genes **NOT** identified as direct *APOLO* targets	AT1G02900	***RALF1***	chr1:653764-654343	WT	*35S:APOLO*	OK	6,43265	11,7847	0,87343	2,3996	0,0001	0,00067	yes
	AT1G12040	***LRX1***	chr1:4070123-4072567	WT	*35S:APOLO*	OK	0,254515	2,57012	3,33601	6,95711	5,00E-05	0,00035	yes
	AT1G12560	***EXPA7***	chr1:4276518-4277899	WT	*35S:APOLO*	OK	0,373865	2,37379	2,6666	4,34024	5,00E-05	0,00035	yes
	AT1G12950	***RSH2***	chr1:4419769-4422638	WT	*35S:APOLO*	OK	0,312439	1,50467	2,2678	4,34933	5,00E-05	0,00035	yes
	AT1G16440	***RSH3***	chr1:5615814-5617672	WT	*35S:APOLO*	OK	0,16653	0,405508	1,28395	1,77649	0,00455	0,01897	yes
	AT1G27740	***RSL4***	chr1:9654687-9656089	WT	*35S:APOLO*	OK	0,105364	0,682308	2,69504	3,06432	0,0005	0,00284	yes
	AT1G32640	***MYC2***	chr1:11798809-11800988	WT	*35S:APOLO*	OK	22,203	52,6239	1,24496	5,66997	5,00E-05	0,00035	yes
	AT2G35150	***PHI-1-like***	chr2:14817046-14818211	WT	*35S:APOLO*	OK	0,264466	1,09189	2,04567	3,08494	5,00E-05	0,00035	yes
	AT1G54970	***PRP1***	chr1:20504999-20506488	WT	*35S:APOLO*	OK	1,07342	8,36667	2,96244	7,31633	5,00E-05	0,00035	yes
	AT1G55330	***AGP21***	chr1:20648464-20648891	WT	*35S:APOLO*	OK	36,0237	97,1117	1,4307	5,34932	5,00E-05	0,00035	yes
	AT1G63450	***RHS8***	chr1:23531408-23534569	WT	*35S:APOLO*	OK	0,03899	0,331918	3,08967	3,72534	5,00E-05	0,00035	yes
	AT1G70460	***PERK13***	chr1:26555845-26559284	WT	*35S:APOLO*	OK	0,258225	1,21635	2,23585	4,60468	5,00E-05	0,00035	yes
	AT2G25260	***HPAT2***	chr2:10755523-10757772	WT	*35S:APOLO*	OK	0,529251	1,33354	1,33324	2,44251	5,00E-05	0,00035	yes
	AT2G43150	***EXT21***	chr2:17945769-17947032	WT	*35S:APOLO*	OK	52,0807	114,204	1,1328	5,20396	5,00E-05	0,00035	yes
	AT2G47540	***SHV2***	chr2:19505859-19506598	WT	*35S:APOLO*	OK	1,0193	4,80441	2,23678	4,04873	5,00E-05	0,00035	yes
	AT3G07340	***bHLH62 TF***	chr3:2340898-2343470	WT	*35S:APOLO*	OK	3,61588	7,57866	1,06759	3,73419	5,00E-05	0,00035	yes
	AT3G10710	***RHS12***	chr3:3352288-3354237	WT	*35S:APOLO*	OK	0,11403	1,03108	3,17667	4,47911	5,00E-05	0,00035	yes
	AT3G21180	***ACA9***	chr3:7425518-7432200	WT	*35S:APOLO*	OK	0,058342	0,415952	2,83382	4,24417	5,00E-05	0,00035	yes
	AT3G28550	***EXT16***	chr3:10688322-10703976	WT	*35S:APOLO*	OK	3,33615	28,0079	3,06958	5,7735	5,00E-05	0,00035	yes
	AT3G43960	***RDL3***	chr3:15774054-15775657	WT	*35S:APOLO*	OK	1,63093	3,72675	1,19223	3,00585	5,00E-05	0,00035	yes
	AT3G48340	***CEP2***	chr3:17897738-17899208	WT	*35S:APOLO*	OK	1,69325	11,8683	2,80925	7,74503	5,00E-05	0,00035	yes
	AT3G54580	***EXT17***	chr3:20200687-20203782	WT	*35S:APOLO*	OK	2,80301	22,185	2,98453	11,514	5,00E-05	0,00035	yes
	AT3G60330	***HA7***	chr3:22297406-22303673	WT	*35S:APOLO*	OK	0,75475	1,83265	1,27986	3,54359	5,00E-05	0,00035	yes
	AT3G62680	***PRP3***	chr3:23182721-23183994	WT	*35S:APOLO*	OK	1,90231	17,1835	3,1752	9,02884	5,00E-05	0,00035	yes
	AT4G02270	***RHS13***	chr4:992174-993038	WT	*35S:APOLO*	OK	0,956108	7,16393	2,90551	5,80735	5,00E-05	0,00035	yes
	AT4G17215	***Pollen Ole e 1 allergen and extensin***	chr4:9655836-9656577	WT	*35S:APOLO*	OK	1,17841	4,76508	2,01566	3,84981	5,00E-05	0,00035	yes
	AT4G22080	***RHS14***	chr4:11700554-11702666	WT	*35S:APOLO*	OK	0,059309	0,757044	3,67406	3,68273	0,00025	0,00154	yes
	AT4G25400	***bHLH TF***	chr4:12981294-12982468	WT	*35S:APOLO*	OK	1,35187	4,32603	1,67809	3,18257	5,00E-05	0,00035	yes
	AT4G29180	***RHS16***	chr4:14385592-14389689	WT	*35S:APOLO*	OK	0,099263	0,521194	2,39249	3,82728	5,00E-05	0,00035	yes
	AT4G29930	***bHLH TF***	chr4:14644008-14647591	WT	*35S:APOLO*	OK	2,30654	7,32455	1,66701	4,31108	5,00E-05	0,00035	yes
	AT4G33880	***RSL2***	chr4:16239362-16241137	WT	*35S:APOLO*	OK	0,038579	0,306499	2,99001	2,43441	0,0083	0,03137	yes
	AT4G36930	***SPT***	chr4:17414126-17416294	WT	*35S:APOLO*	OK	1,36121	2,40537	0,82137	2,05934	0,00055	0,00309	yes
	AT5G05500	***MOP10***	chr5:1629666-1630396	WT	*35S:APOLO*	OK	0,56784	5,15021	3,18108	5,39453	5,00E-05	0,00035	yes
	AT5G19560	***ROPGEF10***	chr5:6603290-6606448	WT	*35S:APOLO*	OK	0,058391	0,406499	2,79944	2,91293	0,0004	0,00233	yes
	AT5G22410	***RHS18***	chr5:7426313-7427964	WT	*35S:APOLO*	OK	0,342718	3,78832	3,46647	6,35329	5,00E-05	0,00035	yes
	AT5G35190	***EXT13***	chr5:13434180-13435167	WT	*35S:APOLO*	OK	1,52769	15,7388	3,3649	8,58919	5,00E-05	0,00035	yes
	AT5G41315	***GL3***	chr5:16529454-16532879	WT	*35S:APOLO*	OK	0,235867	0,44781	0,92491	1,51906	0,0112	0,04019	yes
	AT5G51060	***RHD2***	chr5:20752999-20762431	WT	*35S:APOLO*	OK	0,213913	1,38566	2,69548	3,1665	0,0001	0,00067	yes
	AT5G51790	***bHLH120 TF***	chr5:21039510-21041446	WT	*35S:APOLO*	OK	2,80331	7,68882	1,45563	2,87659	5,00E-05	0,00035	yes
	AT5G54380	***THE1***	chr5:22077059-22080338	WT	*35S:APOLO*	OK	19,729	40,4626	1,03627	4,68266	5,00E-05	0,00035	yes
	AT5G58010	***LRL3***	chr5:23483544-23484889	WT	*35S:APOLO*	OK	0,163107	1,32569	3,02286	3,78898	5,00E-05	0,00035	yes
	AT5G67400	***RHS19***	chr5:26894855-26896488	WT	*35S:APOLO*	OK	0,319731	2,96103	3,21117	5,60471	5,00E-05	0,00035	yes

Supplementary Table 3

	3C-qPCR		Experiment
AT1G66470 *RHD6*	F	TCCCGATTCTTCCCTTAAAAA	3C
	R	AAAGCAAACCTTGGCTGCTA	
	F	AATGACCATCCCAACGAGAC	ChIRP, RT-qPCR
	R	CATAAGCTGCATCTGGCTGA	
	F	GGATTAGAAAGACCAGCTGCTTTAG	ChIP
	R	CCAGTTTGTGAACGACGACA	
AT2G34655 *APOLO*	F	CTTCGAGGCGCTAAACAATC	RIP, RT-qPCR
	R	ACAGCGGTGCCACCTATTAC	
AT5G50300 *AZG2*	F	GGGAGTTGCAAAATGGCTTA	ChIP
	R	CCGACCATGTGAAAAATTCC	
AT4G04450 *WRKY42*	F	CCGCTAAACGCTGGTGAGA	RT-qPCR
	R	CGGCAAAGTTGGGATTGG	
	SALK_049063_LP2	AAGCACGCTTCGATATCTGAG	genotyping
	SALK_049063_RP2	AGTTGCGACAATCAATGGATC	
	SALK_049063_LP4	TTTGTGCGTCTGTTACGTACG	
	SALK_049063_RP4	GTACTTGCTTGCGAACAGGAC	
	F	CACCATGTTTCGTTTTCCGGTAAGTC	cloning
	R	TTGCCTATTGTCAACGTTGCTC	
AT1G13320 Housekeeping 1	F	TAACGTGGCCAAAATGATGC	RIP, RT-qPCR
	R	GTTCTCCACAACCGCTTGGT	

ChIRP 3'BIO probes	
ODD probes	
number	sequence
APOLO 1	aaccagccaatgaacagatg
APOLO 3	gacaagtcacacctacactc
APOLO 5	agttccaaggaatccatacc
APOLO 7	gacagcggtgccacctatta
APOLO 9	ttacaacaagccactccgta
APOLO 11	accaaaacaaccaaaatttt
APOLO 13	ccttacaaacagagcaaagt
APOLO 15	ggaagcaaagcccaaaggaa
APOLO 17	caagtaaccccagaaaacta
APOLO 19	gattccggtgaaatacaagg

EVEN probes	
number	sequence
APOLO 2	gattgtttagcgcctcgaag
APOLO 4	cgagaagaactaggccaaag
APOLO 6	tgaagactaccttacataga
APOLO 8	acaaggaacttccaaccaaa
APOLO 10	caacatctcgtcaaccacat
APOLO 12	cgaaactaaaacaaagaagc
APOLO 14	ggaaataacaaggcaaaaca
APOLO 16	ccgacgattaaaaggataat
APOLO 18	gaaatacaaagccggcggtt
APOLO 20	tcgtctgaaagtttattata

EVEN LacZ probes	
number	sequence
LacZ 1	ccagtgaatccgtaatcatg
LacZ 5	aatgtgagcgagtaacaacc
LacZ 7	aataattcgcgtctggcctt
LacZ 9	aattcagacggcaaacgact
LacZ 11	atcttccagataactgccgt
LacZ 13	gctgatttgtgtagtcggtt
LacZ 15	aactgttacccgtaggtagt
LacZ 17	tttcgacgttcagacgtagt
LacZ 19	accattttcaatccgcacct
LacZ 21	ttcatcagcaggatatcctg